JGR Oceans

RESEARCH ARTICLE
10.1029/2018JC014649

Mechanisms of Ocean Heat Anomalies in the Norwegian Sea

Helene Asbjørnsen[1], Marius Årthun[1], Øystein Skagseth[2], and Tor Eldevik[1]

[1]Geophysical Institute, University of Bergen and Bjerknes Centre for Climate Research, Bergen, Norway, [2]Institute of Marine Research, and Bjerknes Centre for Climate Research, Bergen, Norway

Key Points:
- We document interannual variability of the Norwegian Sea heat content using the ECCOv4 ocean state estimate
- Ocean advection explains the majority of interannual heat content variability in the Norwegian Sea's Atlantic domain
- Ocean advection is related to the Atlantic water inflow strength, and inversely linked to the subpolar gyre strength

Correspondence to:
H. Asbjørnsen,
H.Asbjornsen@uib.no

Citation:
Asbjørnsen, H., Årthun, M., Skagseth, Ø., & Eldevik, T. (2019). Mechanisms of ocean heat anomalies in the Norwegian Sea. *Journal of Geophysical Research: Oceans*, *124*, 2908–2923. https://doi.org/10.1029/2018JC014649

Received 8 OCT 2018
Accepted 2 APR 2019
Accepted article online 10 APR 2019
Published online 29 APR 2019

Abstract Ocean heat content in the Norwegian Sea exhibits pronounced variability on interannual to decadal time scales. These ocean heat anomalies are known to influence Arctic sea ice extent, marine ecosystems, and continental climate. It nevertheless remains unknown to what extent such heat anomalies are produced locally within the Norwegian Sea, and to what extent the region is more of a passive receiver of anomalies formed elsewhere. A main practical challenge has been the lack of closed heat budget diagnostics. In order to address this issue, a regional heat budget is calculated for the Norwegian Sea using the ECCOv4 ocean state estimate—a dynamically and kinematically consistent model framework fitted to ocean observations for the period 1992–2015. The depth-integrated Norwegian Sea heat budget shows that both ocean advection and air-sea heat fluxes play an active role in the formation of interannual heat content anomalies. A spatial analysis of the individual heat budget terms shows that ocean advection is the primary contributor to heat content variability in the Atlantic domain of the Norwegian Sea. Anomalous heat advection furthermore depends on the strength of the Atlantic water inflow, which is related to large-scale circulation changes in the subpolar North Atlantic. This result suggests a potential for predicting Norwegian Sea heat content based on upstream conditions. However, local surface forcing (air-sea heat fluxes and Ekman forcing) within the Norwegian Sea substantially modifies the phase and amplitude of ocean heat anomalies along their poleward pathway, and, hence, acts to limit predictability.

1. Introduction

Ocean heat content variability plays an important role in our climate system. In the Arctic-Atlantic region, ocean heat anomalies have been shown to affect sea ice (e.g., Årthun et al., 2012; Yeager et al., 2015), marine ecosystems (Hátún et al., 2009), and potentially also continental climate (Årthun et al., 2017). There is, however, at present neither consensus nor any complete understanding of the mechanisms causing and maintaining such heat anomalies. One primary question regarding the nature of ocean heat anomalies in the North Atlantic is whether the anomalies are related to upstream ocean circulation changes (e.g., Årthun & Eldevik, 2016; Dong & Kelly, 2003; Hátún et al., 2005; Jungclaus et al., 2014; Sutton & Allen, 1997), or whether they are more the surface ocean signature of evolving large-scale atmospheric patterns such as the North Atlantic Oscillation (NAO; Foukal & Lozier, 2016; Krahmann et al., 2001; Saravanan & McWilliams, 1998). Understanding the mechanisms of ocean heat anomalies, with a special emphasis on quantifying the relative influence of ocean advection and air-sea heat fluxes, has implications for climate predictability, as heat anomalies caused by ocean circulation changes appear more predictable than those caused by surface heat fluxes (Yeager & Robson, 2017).

The Norwegian Sea (Figure 1a) is a key component of the North Atlantic climate system, as it acts as a transition zone between the temperate North Atlantic and the cold Arctic Ocean. The oceanographic conditions are influenced by the northward flowing Norwegian Atlantic Current (NwAC) transporting warm, saline Atlantic water into the region (Orvik & Niiler, 2002; Skagseth et al., 2008). After entering the Norwegian Sea, the Atlantic water is modified along its poleward pathway due to heat loss to the atmosphere and lateral eddy exchanges with the colder and fresher Greenland and Iceland Seas (Chafik et al., 2015; Furevik, 2001; Segtnan et al., 2011). In leaving the Norwegian Sea, parts of the Atlantic water will enter the Barents Sea and the Arctic Ocean through the Barents Sea Opening (BSO) and the Fram Strait respectively, and parts will recirculate within the Nordic Seas (Eldevik et al., 2009; Skagseth et al., 2008).

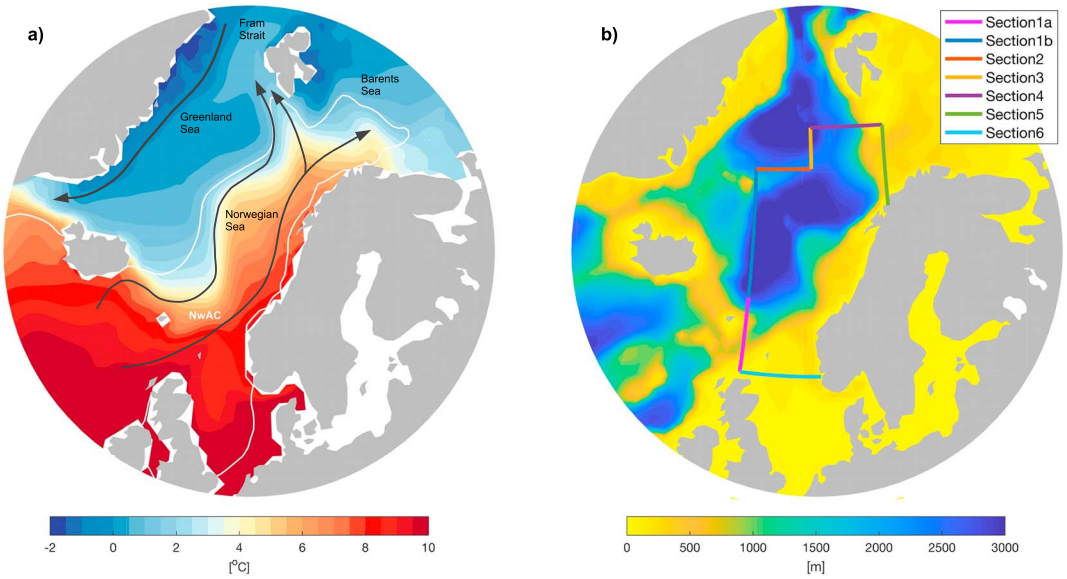

Figure 1. North Atlantic-Nordic Seas temperature and bathymetry. (a) Upper-ocean (0–350 m) mean potential temperature and 35 isohaline (white contour line), with main circulation features indicated. (b) Ocean depth, with Norwegian Sea domain boundary Sections1–6 marked. NwAC = Norwegian Atlantic Current.

Heat exchanges between the Norwegian Sea and neighboring oceans have been studied ever since the first budget estimate was put forward by Mosby (1962). While early work (as summarized in Simonsen & Haugan, 1996) was based on mean ocean transports to and from the Nordic Seas, more recent budget studies have additionally applied atmospheric reanalysis fields to estimate mean heat exchanges with the atmosphere (Segtnan et al., 2011; Simonsen & Haugan, 1996). An alternative approach has been to use air-sea heat fluxes from atmospheric reanalysis together with ocean heat content from hydrography and calculate the ocean heat transport component as a residual (Carton et al., 2011; Mork et al., 2014), something which allows for heat content changes to be assessed.

The Norwegian Sea exhibits pronounced variability in ocean heat content on interannual to decadal timescales. It is, however, not known to what extent the region is a passive receiver of heat anomalies formed elsewhere and to what extent the anomalies are produced locally, for instance, by anomalies in the regional atmospheric circulation (Lien et al., 2014), or a varying influence of the East Icelandic Current (Mork et al., 2014). Focusing on the Atlantic domain of the Nordic Seas, Carton et al. (2011) find ocean advection to be the dominant cause of interannual to decadal heat content variability for the time period 1950–2009, with local air-sea heat fluxes only having a weak reinforcing effect on the anomalies. Mork et al. (2014), on the other hand, find local air-sea heat fluxes to explain about half of the observed heat content variability in the Norwegian Sea between 1951 and 2010. However, these studies, based on comparisons between observed heat content variations (from hydrography) and air-sea fluxes from different reanalysis products, suffer from the inability to close the heat budget, as ocean heat transport is not a well-observed quantity. The role of ocean advection in observation-based studies can therefore only be obtained as a residual, and a detailed examination of the relative contributions of ocean dynamics and local surface forcing has yet to be performed.

In this paper we identify the mechanisms responsible for ocean heat content variability in the Norwegian Sea, using the physically consistent ECCOv4 ocean state estimate (Forget et al., 2015a; Fukumori et al., 2017; Wunsch & Heimbach, 2007). First, we quantify the contribution from air-sea heat fluxes and ocean advection. Then, the contribution of ocean advection is elucidated in more detail by exploring the relative importance of resolved (Eulerian) and eddy-driven (bolus) advection in driving ocean heat transport convergences, as well as the importance of wind-driven Ekman dynamics. A temporal and spatial decomposition furthermore identifies the main sources of advective heat transport variability. Finally, we assess the dominant large-scale oceanic and atmospheric circulation anomalies associated with a variable heat transport to the Norwegian Sea.

2. Methods

2.1. ECCOv4 Ocean State Estimate

ECCO version 4 release 3 (hereafter referred to as ECCOv4) is an ocean state estimate of the 1992–2015 global ocean circulation and sea ice state, generated by fitting the Massachusetts Institute of Technology General Circulation Model (MITgcm) to satellite and in situ ocean observations in a least square sense (Forget et al., 2015a; Fukumori et al., 2017; Wunsch & Heimbach, 2007). The ocean-ice component of the MITgcm produces monthly fields by solving the primitive equations for a time-evolving, Boussinesq, hydrostatic ocean with a nonlinear free surface. Through the adjoint method (Heimbach et al., 2005), these model fields are constrained by ocean observations. Latent, sensible, and upward radiative heat fluxes are calculated from bulk formulae (Large & Yeager, 2004), with ERA-Interim reanalysis (Dee et al., 2011) used as the initial near surface atmospheric state (air temperature, humidity, precipitation, downward radiation, and wind stress). The MITgcm framework obeys the conservation laws of momentum, mass, heat, and salt, and the adjoint method avoids adding nonphysical source/sink terms to the model equations. Consequently, the ECCOv4 estimate is dynamically and kinematically consistent and allows for closed heat, salt, and volume budgets at each grid cell, to machine precision (Buckley et al., 2014, 2015; Piecuch et al., 2017).

The ECCOv4 state estimate is gridded at a LLC90 grid—a global lon-lat-cap (LLC) grid split into five "gcm-faces," one of which is the "Arctic cap" (Forget et al., 2015a). The four grid vertices of the Arctic cap are placed over land at 67°N, while for Antarctica two grid vertices are placed over land at 80°S and away from major ice shelves. The grid has a 1° nominal horizontal resolution, and 50 unevenly spaced vertical layers. The meridional resolution in the Norwegian Sea region is approximately 0.5°, which is larger than the internal deformation radius (Nurser & Bacon, 2014) and the dominant eddy scale (Poulain et al., 1996). The effect of unresolved mesoscale eddies is parameterized as a bolus velocity (Gent & Mcwilliams, 1990). Time-invariant three-dimensional turbulent transport parameters, such as the Gent-McWilliams bolus velocity (eddy) coefficient, are estimated within the ECCOv4 framework under the constraints of observations (Forget et al., 2015a). Constraining the turbulent transport parameters in ECCOv4 greatly improves the fit to in situ profiles compared to earlier ECCO solutions (Forget et al., 2015b).

2.2. Comparison to Observations

In combining the physical consistency of a GCM with actual observational data, ECCOv4 is ideal for a regional heat budget analysis of the Norwegian Sea. To test ECCOv4's general applicability for the Nordic Seas region, we compare to observed ocean heat and freshwater anomalies from the combined data sets of the Institute of Marine Research, the Polar Research Institute of Marine Fisheries and Oceanography, and the Argo Global Data Assembly Centre (Coriolis Data Centre), acquired from the ICES Report on Ocean Climate (González-Pola et al., 2018). The ECCOv4 heat and freshwater content is calculated by integrating temperature and freshwater (relative to a reference salinity of 34.8) over the Norwegian Sea domain seen in Figure 1b. The observed heat and freshwater content is an estimate over the Atlantic water layer of the topographically defined Norwegian Sea domain seen in Mork et al. (2014; mean Atlantic water depth between 1951 and 2010 is 409 m). We note, however, that the comparison is not sensitive to the exact definition of our domain.

The overall variability in heat and freshwater content for the 1992–2015 period is captured well by the ECCOv4 estimate (Figure 2; $r = 0.87$ for the upper 400 m). ECCOv4 does, however, appear slightly colder and fresher than the observations. Another noticeable difference is the delayed late 1990s warming trend in ECCOv4. Still, the comparison to hydrography is favorable, though not entirely surprising, as ECCOv4 is constrained to some of the same observational data (e.g., Argo data).

We furthermore compare temperature and volume transport estimates in ECCOv4 to observations from the Faroe-Shetland Channel (FSC; available from the ICES Report on Ocean Climate and Marine Scotland, UK, respectively) and the BSO (provided by the Institute of Marine Research, Norway). As seen in Figures 3c and 3d, the observed temperature compares well with the ECCOv4 estimate for both the FSC and the BSO. While the time-mean volume transport at the BSO is captured accurately by ECCOv4 (Figure 3b; 2.0 versus 2.1 Sv in observations), the interannual variability is not reproduced. The low correlation could, in part, be a result of insufficient horizontal resolution in both current measurements (Ingvaldsen et al., 2002) and ECCOv4, neither being able to resolve the internal radius of deformation in the BSO (Nurser & Bacon, 2014). We note that high-resolution (1/4°-4 km) ocean models also struggle to capture observed volume

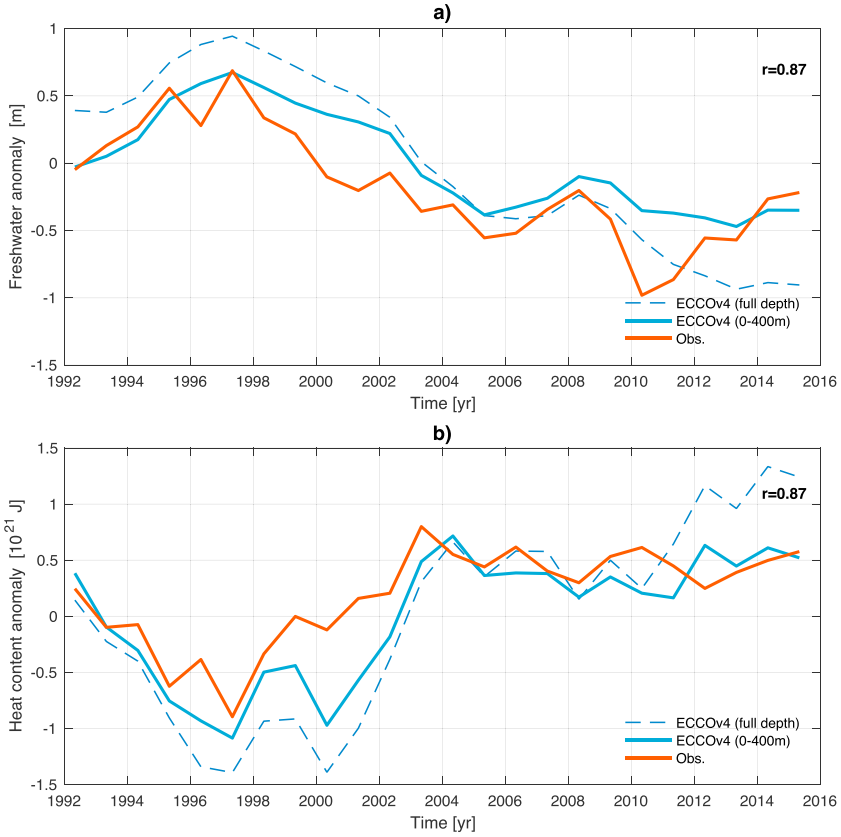

Figure 2. Comparison to hydrography. (a) May freshwater anomaly for the Norwegian Sea in ECCOv4 relative to 34.8, and May-centered freshwater anomaly for the Norwegian Sea Atlantic water layer in observations. (b) May heat content anomaly for the Norwegian Sea in ECCOv4, and May-centered heat content anomaly for the Norwegian Sea Atlantic water layer in observations. Correlations between the observations and the 0–400 m anomaly in ECCOv4 is noted in the upper right-hand corner. May-centered hydrography stems from annual internationally coordinated cruises between 15 April and 15 June and is acquired from the ICES Report on Ocean Climate.

transport variations in the BSO (Lien et al., 2016). The transport of Atlantic water through the FSC is, on the other hand, reproduced well by ECCOv4 (Figure 3a; $r = 0.68$). As the inflow through the FSC is the main provider of Atlantic heat to the Norwegian Sea, these results (Figures 3a and 3c), together with the favorable comparison to observed hydrography (Figure 2), provide confidence in the ability of ECCOv4 to assess ocean heat content variability in the Norwegian Sea, and its drivers.

2.3. Heat Budget

In order to identify the processes driving interannual heat content variability in the Norwegian Sea, a regional heat budget is calculated using the ECCOv4 ocean state estimate. The Norwegian Sea domain (Figure 1b) is enclosed by six boundary sections plus the Norwegian coast as the eastern boundary. Section1 is split into two parts and will be treated separately, as the inflow of warm Atlantic water occurs in Section1's southernmost part (Section1a; 6.1 Sv in), while small amounts of relatively cold water is exiting the domain through the northernmost part (Section1b; 0.6 Sv out). The northern section toward the Fram Strait (Section4; 8.2 Sv out) and the section at the BSO (Section5; 3.3 Sv out) are the main outflow regions where warm Atlantic water exits the Norwegian Sea domain and continues toward the Arctic (Figure 1a). Although the locations of the defined boundary sections make them not directly comparable to observations from the Fram Strait and the BSO, we note that the simulated transports toward the Arctic are in broad agreement with observational estimates (Schauer et al., 2004; Skagseth et al., 2008).

The heat content tendency for a given control volume is determined by convergence of advective, diffusive, and surface heat fluxes. The heat budget equation describing this relationship, originates from integrating

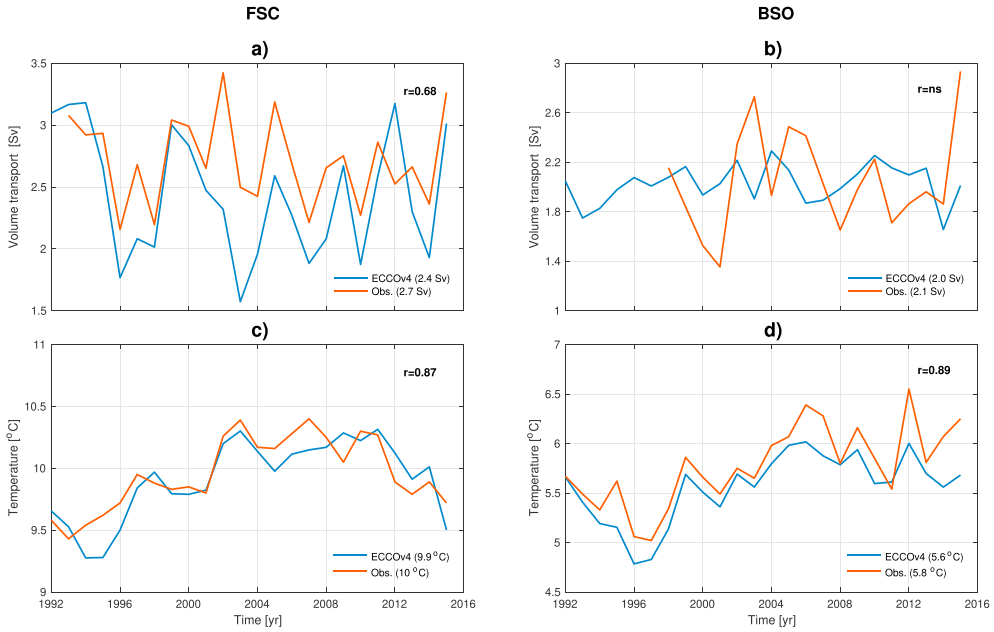

Figure 3. Comparison to observations. Annual mean volume transport in (a) the Faroe-Shetland Channel (Berx et al., 2013), and (b) the Barents Sea Opening (Skagseth et al., 2008), from observations and ECCOv4. Annual mean temperature at (c) the Faroe-Shetland Channel (0–200 m), and (d) the Barents Sea Opening (50–200 m), in observations (ICES Report on Ocean Climate) and ECCOv4. The time-mean volume transport (a, b) and temperature (c, d) are noted in parentheses in the lower right-hand corner. Correlations between the respective time series are noted in the upper right-hand corner ("ns" stands for "not significant").

the conservation of heat equation over a chosen geometric volume V:

$$\underbrace{\rho_o C_p \iiint_V \frac{\partial \theta}{\partial t} \mathrm{d}V}_{Tend} = \underbrace{\rho_o C_p \iiint_V (-\nabla \cdot \mathbf{u}\theta) \mathrm{d}V}_{ADV} + \underbrace{\rho_o C_p \iiint_V (-\nabla \cdot \mathbf{K}) \mathrm{d}V}_{DIFF} + \underbrace{\rho_o C_p \iiint_V Q \mathrm{d}V}_{Qnet} \quad (1)$$

where ρ_o is a reference density of seawater, C_p is the specific heat capacity, θ is potential temperature, $\mathbf{u}$ is the three-dimensional velocity vector, $\mathbf{K}$ is the diffusive temperature flux vector, and Q is the net air-sea heat flux (sensible, latent, shortwave, and longwave). For conceptual and methodological simplicity and robustness, for example, to avoid effects of local vertical heaving, we choose to integrate the Norwegian Sea domain from the sea surface to the ocean bottom. However, we note that the heat budget is dominated by upper-ocean variability (Figure 2b). The budget terms will for simplicity be referred to as heat content tendency *Tend*, advective heat transport convergence *ADV*, diffusive heat transport convergence *DIFF*, and net air-sea heat fluxes *Qnet*.

Following the approach and terminology of Piecuch and Ponte (2012), we use "Variance Explained" (ν) as a metric to quantify the amount of variability in heat content tendency *Tend* explained by the respective budget terms:

$$\nu(x, y) = 100\% \times \left(1 - \frac{\sigma^2(x - y)}{\sigma^2(x)}\right), \quad (2)$$

where σ^2 is the temporal variance. The $\nu(x, y)$ takes on values between $-\infty$ and 100 and gives the percentage of variance in variable x explained by variable y. A value of, for example, 40% indicates that 40% of the variance in x can be explained by variance in y, while a value of -40% means that the variance in y increases the variance in x by 40%. Large negative values ($< -100\%$) indicate that the signals are out of phase and/or that the variance in y is larger than the variance in x. Applying the metric to our heat budget ($Tend = ADV + DIFF + Qnet$), x equals the heat content tendency *Tend* and y equals one of the remaining budget terms, depending on which one is being analyzed.

In order to explore the link between Atlantic water inflow and large-scale atmospheric forcing, the leading modes of atmospheric variability for the ECCOv4 time period (1992–2015) are identified by calculating

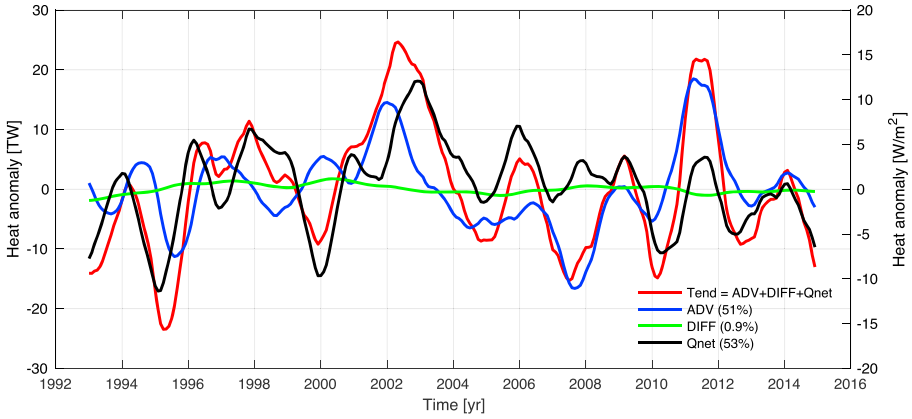

Figure 4. Norwegian Sea heat budget. Deseasoned, detrended, and 1-year low-pass-filtered heat budget (1993–2014) for the Norwegian Sea domain, where *Tend* is the heat content tendency, *ADV* is the advective heat transport convergence, *DIFF* is the diffusive heat transport convergence, and *Qnet* is the net air-sea heat fluxes; 1 TW equals 10^{12} J/s. Variance in *Tend* explained by the respective budget terms is noted in parentheses.

empirical orthogonal functions for area-weighted sea level pressure over the North Atlantic region, using the original ERA-Interim reanalysis fields used to force the MITgcm (the adjusted fields are not available as output). The two leading modes are the NAO (41% of the variance) and the East Atlantic Pattern (EAP; Barnston and Livezey (1987); 17% of the variance). NAO and EAP indexes are defined using the principal component time series. Our empirical orthogonal function-based NAO index is strongly correlated ($r = 0.85$) with the station-based index of Hurrell (1995).

As we focus on interannual variability, seasonal cycles and linear trends are removed from all time series from here and onward. In order to accentuate interannual variability, the time series are smoothed by applying a 1-year low-pass triangular filter (24-month filter width). To avoid edge effects from filtering, the first and last 12 months of the time series are removed, leaving us with the 1993–2014 time period that will be analyzed here.

3. Results

3.1. Norwegian Sea Heat Budget

The Norwegian Sea heat budget shows pronounced interannual variability, with standard deviations of 10.3 TW for *Tend*, 6.8 TW for *ADV*, 7.1 TW for *Qnet*, and 0.8 TW for *DIFF* (Figure 4). Fifty-one percent of the variability in *Tend* is explained by variability in *ADV*, and 53% is explained by variability in *Qnet*. *DIFF* is practically negligible, explaining only 0.9% of the variability. These results translate to an equal contribution from ocean advection and air-sea heat fluxes in driving the interannual Norwegian Sea heat content variability, consistent with the findings of Mork et al. (2014).

While *ADV* and *Qnet* are found to be equally important when integrating the heat budget over the Norwegian Sea domain in its entirety, this does not exclude the possibility of large spatial variations in the importance of the individual budget terms. Consequently, a spatial analysis is carried out by calculating the depth-integrated heat budget for each horizontal grid cell within the Norwegian Sea domain and neighboring areas, and mapping the relative importance of the budget terms (Figure 5). Note that summing the depth-integrated budgets within the Norwegian Sea domain gives the volume-integrated budget in Figure 4.

Figure 5a shows pronounced spatial variations in the ability of *ADV* to explain the variability in *Tend*. Toward the center of the Norwegian Sea domain (southwest to northeast), *ADV* explains the majority of the variability in *Tend* (60–80%). This area largely coincides with the extent of the Atlantic water (defined here as the horizontal area with salinity ≥35 in the upper 350 m within the Norwegian Sea domain), along which *ADV* explains 62% and *Qnet* 39% of the interannual heat content variability. A branching pattern is also visible at the northern boundary, indicating that heat content variability along the NwAC is closely related to advective heat transport. As *ADV* and *Tend* are largely positively correlated (Figure 5b), areas with large negative ν values are generally due to a larger temporal variance σ^2 in *ADV* compared to that in *Tend* (equation (2)).

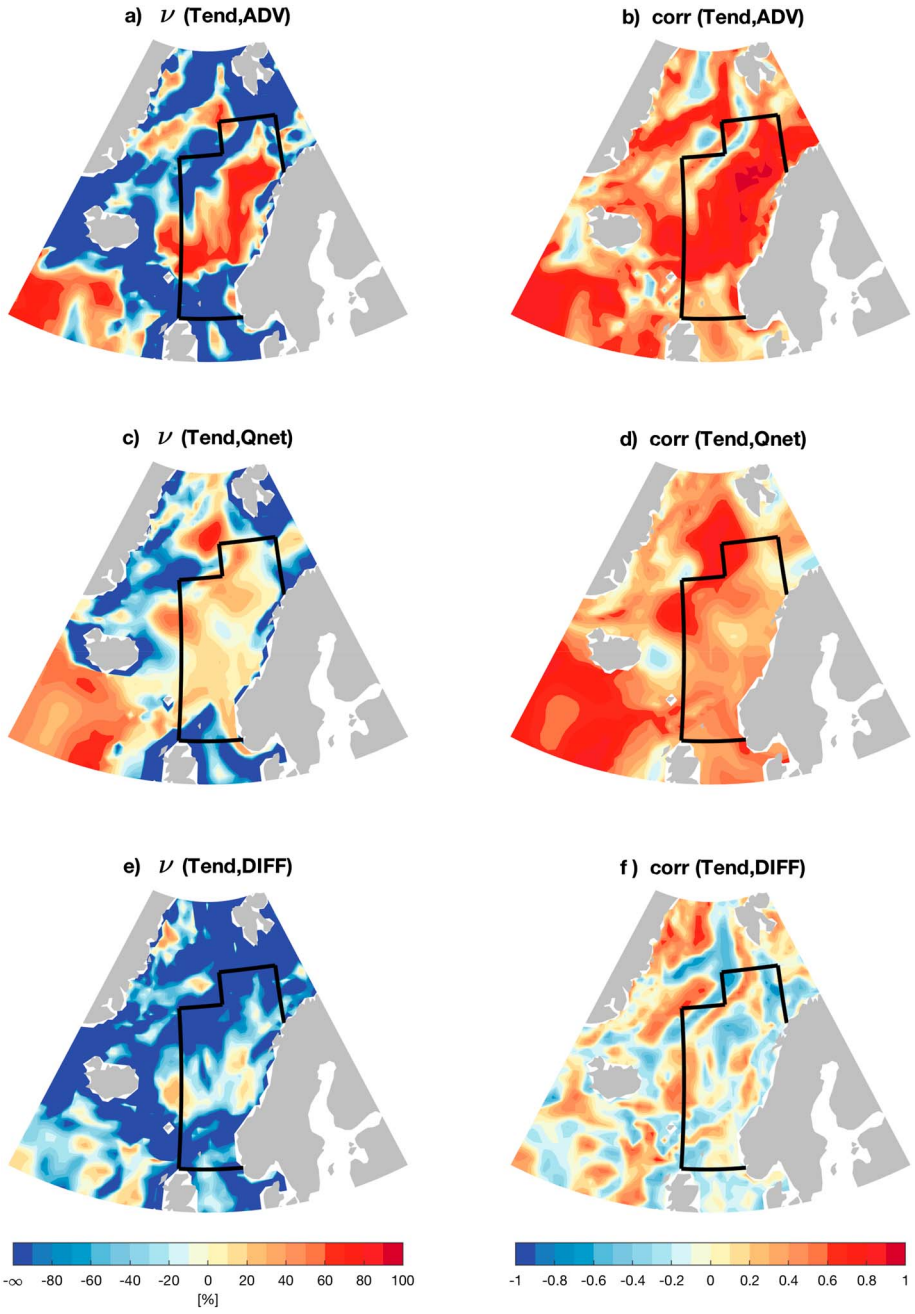

Figure 5. Spatial heat budget analysis. (a, c, and e) Variance in *Tend* explained by respective budget terms in each horizontal grid cell, and (b, d, and f) correlation between *Tend* and respective budget terms. The analysis is based on deseasoned, detrended, and 1-year low-pass-filtered depth-integrated heat budgets. The Norwegian Sea domain is indicated by the solid black lines.

A noticeable feature in Figure 5a is the discontinuity at the Iceland-Scotland Ridge, separating high ν values in the subpolar North Atlantic and within the Nordic Seas. The Atlantic inflow across the ridge takes place through narrow channels, and the flow is characterized by high mesoscale activity, leading to high transport variability (Sherwin et al., 2006; Zhao et al., 2018). Closer inspection of the region shows that the discontinuity in ν values across the ridge is much reduced if we consider unfiltered monthly time series. While exchanges between the Norwegian Sea and the North Atlantic south of the ridge are observed to occur on a broad range of time scales (Bringedal et al., 2018; Hansen & Østerhus, 2000), the processes driving local heat content change at the ridge is thus found to act predominantly on subannual time scales.

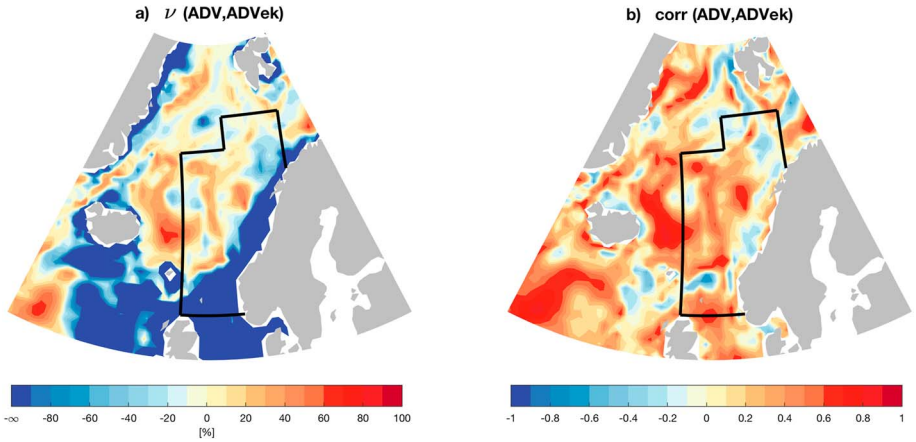

Figure 6. Role of Ekman forcing. (a) Variance in *ADV* explained by Ekman forcing ADV_{ek} in each horizontal grid cell, and (b) correlation between *ADV* and ADV_{ek}. The analysis is based on deseasoned, detrended, and 1-year low-pass-filtered depth-integrated heat budgets. The Norwegian Sea domain is indicated by the solid black lines.

Within the Norwegian Sea domain, *Qnet* is positively correlated to *Tend* (Figure 5d), though the correlations are slightly weaker compared to *ADV* (Figure 5b). Figure 5c shows higher ν values in the eastern Nordic Seas, compared to the western Nordic Seas, implying that air-sea heat fluxes acts as a source of interannual heat content variability throughout the Norwegian Sea domain.

The ability of *DIFF* to explain variability in *Tend* is modest (Figure 5e). Figure 5f shows a highly fractioned spatial pattern, with the highest correlations near the northwestern boundaries of the Norwegian Sea domain, something which could be related to lateral heat loss from the warm NwAC by isopycnal diffusion observed in the region (e.g., Isachsen et al., 2012; Nilsen et al., 2006).

3.2. Role of Local Wind Forcing

Ocean advection appears to be the dominant driving mechanism of ocean heat content variability in the Atlantic domain within the Norwegian Sea domain. However, some fraction of this advective heat transport variability is likely directly attributable to local wind forcing (Ekman forcing). In order to quantify this contribution, we calculate the advective heat transport convergence by Ekman transport ADV_{ek}.

Following the approach of Buckley et al. (2014), we assume that the horizontal velocity $\mathbf{u_h}$ can be decomposed into a geostrophic part $\mathbf{u_g}$ and an Ekman part $\mathbf{u_{ek}}$: $\mathbf{u_h} \approx \mathbf{u_g} + \mathbf{u_{ek}}$. The horizontal Ekman velocity is given by

$$\mathbf{u_{ek}} = \frac{\mathbf{M_{ek}}}{D_{ek}} = \frac{\boldsymbol{\tau} \times \hat{\mathbf{z}}}{\rho_o f D_{ek}} \tag{3}$$

where $\mathbf{M_{ek}}$ is the Ekman transport, D_{ek} is the Ekman depth (here 50 m is used; e.g., Rio & Hernandez, 2003), τ is the wind stress, and f is the Coriolis parameter. The vertical Ekman transport vanishes, as we consider the full ocean depth. Advective heat transport convergence by Ekman transport for a horizontal grid cell is then given by

$$ADV_{ek} = \rho_o C_p \int_{-D_{ek}}^{\eta} (-\nabla \cdot \bar{\mathbf{u}}_{\mathbf{ek}} \bar{\theta}) \mathrm{d}z \tag{4}$$

where $\bar{\mathbf{u}}_{\mathbf{ek}}$ and $\bar{\theta}$ is the time-evolving Ekman velocity and potential temperature, averaged over the Ekman layer. The lack of difference between using time-evolving $\bar{\theta}$ and climatological $\bar{\theta}$ (not shown), indicates that local wind variability dominates over temperature field changes in causing interannual variability in ADV_{ek}. The shallow areas along the Norwegian coast and at the southern boundary (Figure 1b) will not be discussed, as the approximation $\mathbf{u_h} \approx \mathbf{u_g} + \mathbf{u_{ek}}$ breaks down for shallow regions due to lateral friction and bottom Ekman layers (Buckley et al., 2014).

Figure 6 shows that *ADV* and ADV_{ek} are largely positively correlated, and ADV_{ek} is found to contribute to interannual variability in *ADV* toward the center of the Norwegian Sea domain, explaining 30–40% or less of the variability. These results suggest that Ekman dynamics is important, but not dominant, in driving

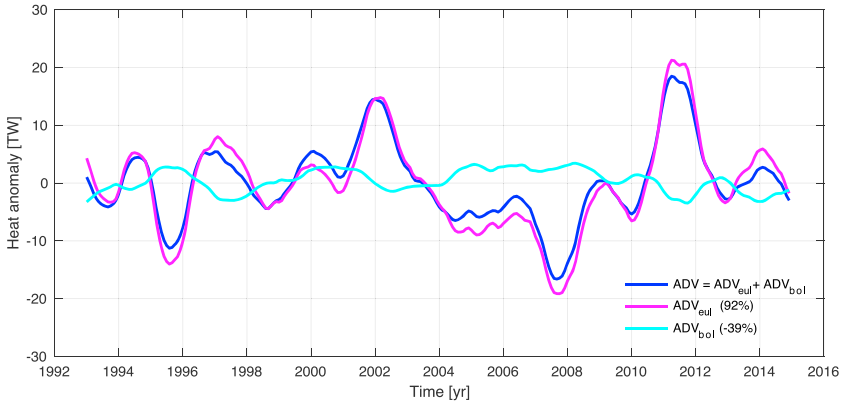

Figure 7. Role of eddy-scale processes. Decomposition of the Norwegian Sea heat budget term *ADV* into advection by resolved (ADV_{eul}) and bolus (ADV_{bol}) velocities. Variance in *ADV* explained by ADV_{eul} and ADV_{bol} is noted in parentheses.

advective heat transport convergence *ADV*. Forcing by local wind variability within the Norwegian Sea particularly acts to enhance the variance of heat anomalies advected into the domain with the North Atlantic Current/NwAC.

3.3. Decomposition of Advection

Advection of heat anomalies into the Norwegian Sea domain has been shown to be a driving mechanism of Norwegian Sea heat content variability comparable in size to that of local surface forcing (air-sea heat fluxes and Ekman forcing). In order further to understand the advection mechanism, spatial and temporal decompositions of the volume-integrated Norwegian Sea heat budget term *ADV* from Figure 4 are now carried out.

3.3.1. Eulerian and Eddy-Driven Advection

Advection by both resolved (Eulerian) and parameterized (bolus) velocities constitute the advective heat transport convergence budget term: $ADV = ADV_{eul} + ADV_{bol}$ (Buckley et al., 2014; Piecuch et al., 2017). Considering the two model velocities separately, we find that *ADV* largely originates from temperature advection by the resolved velocity field ADV_{eul} (Figure 7). The eddy-driven advection ADV_{bol} acts in the opposite direction of ADV_{eul} but has a small magnitude in comparison. ADV_{bol} acting to compensate for ADV_{eul} is consistent with eddies cooling the NwAC by transporting the warm Atlantic water away from the mean current (Isachsen et al., 2012). A stronger Atlantic water current would then imply increased eddy activity, and more heat loss from the Atlantic water core. The importance of eddy exchanges with the colder and fresher neighboring Iceland and Greenland Seas has been highlighted in previous budget studies (Segtnan et al., 2011) and is consistent with ADV_{bol} contributing to heat transport convergence along the northwestern and northern boundaries of our Norwegian Sea domain.

3.3.2. Source of Advective Heat Transport Variability

The heat transport convergence term *ADV* accounts for heat transport variations through six boundary sections encompassing the Norwegian Sea. The sections capture the different branches of the NwAC; the Atlantic water inflow across the Greenland-Scotland Ridge (Section1a; AWin), and the two northern branches entering the Fram Strait (Section4; FS) and the Barents Sea (Section5; BS). By analyzing the importance of the different branches and their driving mechanisms, we aim to identify the source of advective heat transport variability for the Norwegian Sea.

For individual sections where the volume transport is not balanced, heat transport is not well defined (Schauer & Beszczynska-Möller, 2009), but a relative value can be calculated by using a reference temperature. Because we are concerned with the heat transport (*HT*) that actually alters the heat content of the Norwegian Sea domain, we use the time-evolving volume-averaged Norwegian Sea temperature as a reference temperature θ_{ref}, following the approach of Lee et al. (2004):

$$\theta_{ref}(t) = \iiint_V \theta(t,x,y,z)\mathrm{d}V \tag{5}$$

$$HT = \rho_o C_p \int_S (\mathbf{v}\cdot\mathbf{n})(\theta - \theta_{ref})\mathrm{d}S \tag{6}$$

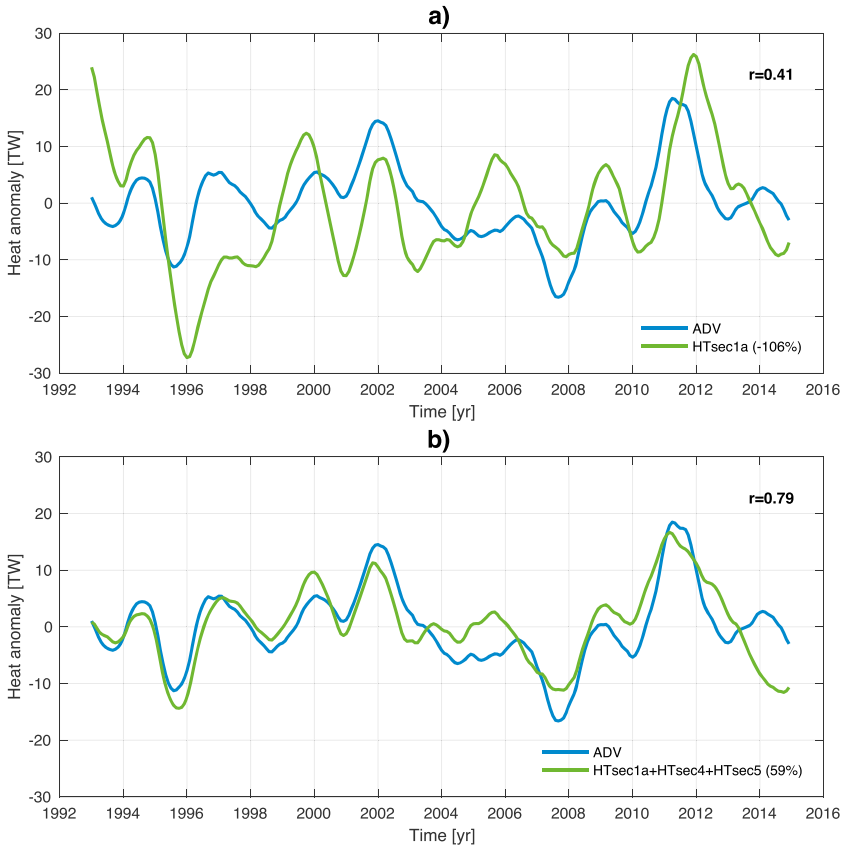

Figure 8. Atlantic water inflow as source of *ADV* variability. Norwegian Sea heat budget term *ADV* versus (a) heat transport through Section1a (AWin), and (b) summed heat transport through Section1a (AWin), Section4 (FS), and Section5 (BS). Heat transport is positive when warm water (relative to θ_{ref}; equation (6)) is brought into, or cold water out of, the Norwegian Sea domain. Correlations are noted in the upper right-hand corner. Variance in *ADV* explained by the heat transport through the respective boundary sections are noted in parenthesis.

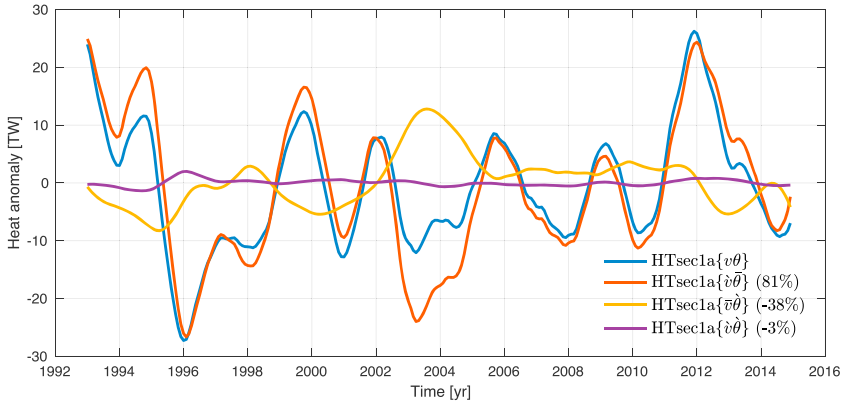

Figure 9. Decomposition of heat transport $HT\{v\theta\}$ through Section1a (AWin) into a velocity component $HT\{v'\bar{\theta}\}$, a temperature component $HT\{\bar{v}\theta'\}$, and a covariance component $HT\{v'\theta'\}$. Heat transport is positive when warm water (relative to θ_{ref}; equation (6)) is brought into, or cold water out of, the Norwegian Sea domain. Variance in $HT\{v\theta\}$ explained by the respective terms is noted in parentheses.

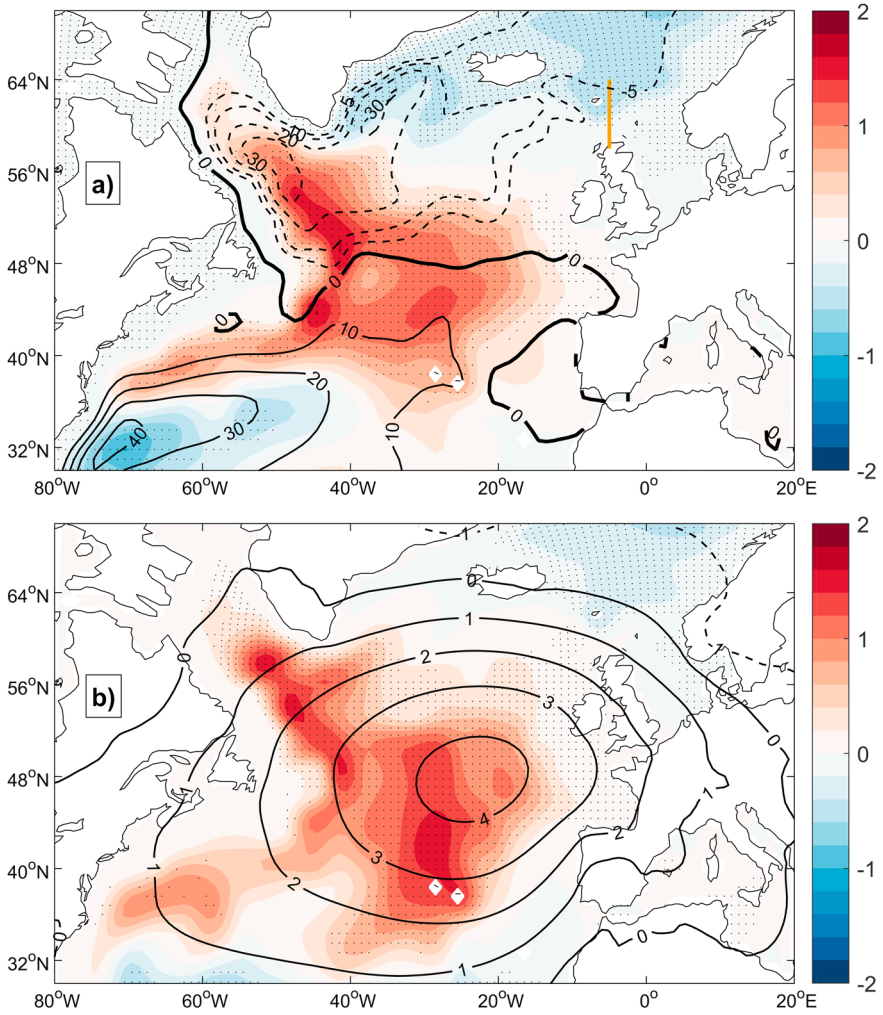

Figure 10. Linear regression between (a) $HT\{v'\bar{\theta}\}$ and the barotropic stream function and (b) between the East Atlantic Pattern and the barotropic stream function (units: Sv/std[index]). All time series were detrended and filtered prior to analysis. In (a) the mean barotropic stream function (Sv) is also shown by the black contours. The subpolar and the subtropical gyres are characterized by cyclonic (negative) and anticyclonic (positive) circulation, respectively. In (b) the black contours show the sea level pressure anomalies (hPa) associated with the East Atlantic Pattern. The location of Section1a (AWin) used to calculate $HT\{v'\bar{\theta}\}$ is shown in (a) by the orange line. Dots indicate where the correlation is significant at the 95% confidence level (Ebisuzaki, 1997).

where V is the Norwegian Sea volume and S is the surface area of the boundary section analyzed. We note that the volume-averaged Norwegian Sea temperature is practically 0 °C, regardless of averaging over the full ocean depth or over the upper ocean (e.g., 0–550 m), or using the corresponding time-mean value. The applied reference temperature is thus close to that used by previous studies on heat transport in the Nordic Seas (e.g., Årthun et al., 2012; Orvik & Skagseth, 2005), and our results are not noticeably sensitive to the assessed methods of choosing θ_{ref}.

The heat transport through Section1a (AWin) is more related to *ADV* ($r = 0.41$; Figure 8a) than any of the other boundary sections (HTsec4 and HTsec5 are not correlated to *ADV*). This supports an important contribution to the Norwegian Sea heat budget from upstream ocean heat anomalies transported by the North Atlantic Current/NwAC. The negative ν value (−106%) arises from HTsec1a having a higher variance than *ADV* (10.3 and 6.8 TW, respectively). To capture the correct phase and amplitude of the basin-scale heat anomalies, it is necessary to include the outflow regions Section4 (FS) and Section5 (BS; Figure 8b). Such a finding highlights the important role of local surface forcing in modifying the heat anomalies within the Norwegian Sea domain (Furevik, 2001).

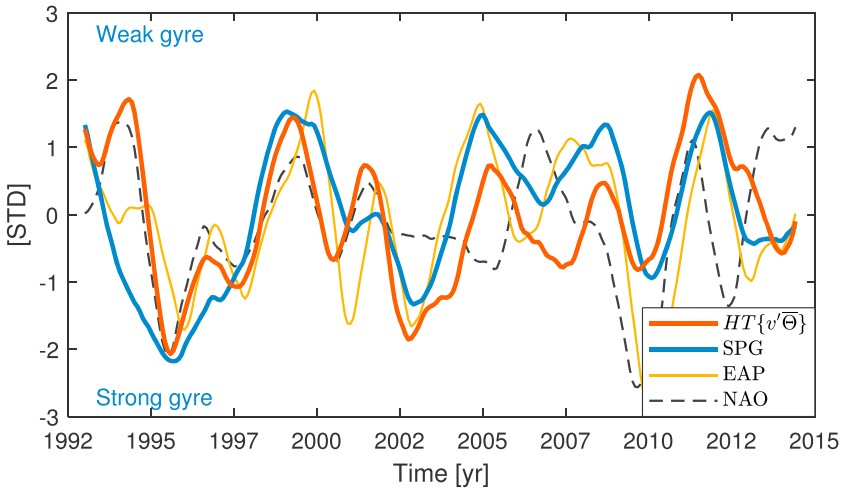

Figure 11. Standardized time series of the Atlantic inflow to the Nordic Seas ($HT\{v'\bar{\theta}\}$), the SPG strength (inverted), and the NAO and EAP indexes (calculated as the principal components of the first two modes of sea level pressure variability). SPG = subpolar gyre; EAP = East Atlantic Pattern; NAO = North Atlantic Oscillation.

In order to determine the driver of Atlantic water inflow variability, a temporal decomposition of the heat transport through Section1a is carried out. The Atlantic water inflow variability can originate from anomalous velocities $\{v'\bar{\theta}\}$, changes in the temperature of the advected water mass $\{\bar{v}\theta'\}$, or the covariance between the two $\{v'\theta'\}$: $HT\{v\theta\} = HT\{v'\bar{\theta}\} + HT\{\bar{v}\theta'\} + HT\{v'\theta'\}$, where overbar denotes the time mean and prime denotes the time anomaly. As seen in Figure 9, the Atlantic water inflow variability is dominated by velocity fluctuations v' (explain 81% of the variability) rather than temperature fluctuations. This is in agreement with observations from the NwAC (Orvik & Skagseth, 2005), and modeled heat transport at the Greenland-Scotland Ridge (Årthun & Eldevik, 2016). For the two outflow regions, the same decompositions show that velocity fluctuations v' play a leading role at Section5 (66%), though temperature fluctuations T' are also important (58%). At Section4, on the other hand, temperature fluctuations T' take the leading role (85%), but with velocity fluctuations v' also being important (42%).

3.3.3. Relation to Large-Scale Forcing

Having identified volume transport fluctuations $HT\{v'\bar{\theta}\}$ in the Atlantic inflow to play a leading role in the Norwegian Sea heat budget, we now aim to identify the dominant mechanisms of anomalous Atlantic water circulation in ECCOv4. To assess the dynamic variations in North Atlantic circulation associated with $HT\{v'\bar{\theta}\}$, Figure 10a shows the regression between $HT\{v'\bar{\theta}\}$ and the barotropic stream function in the North Atlantic. A stronger inflow to the Nordic Seas is associated with a weakened subpolar gyre (SPG) and a strengthening, and northward shift, of the North Atlantic Current that flows along the zero line of the stream function. The covariability between the Atlantic inflow to the Nordic Seas and ocean circulation in the subpolar North Atlantic can be quantified by calculating the SPG strength, defined as the absolute value of the minimum barotropic stream function in the subpolar region. For the time period covered by ECCOv4 the SPG strength shows a good connection to $HT\{v'\bar{\theta}\}$ (r=-0.54), and especially after the late 1990s the covariability is strong (Figure 11). These results support a close coupling between the subpolar North Atlantic and the Nordic Seas (Hátún et al., 2005; Langehaug et al., 2012; Yeager et al., 2015).

The origin of ocean circulation variability in the subpolar North Atlantic has been much studied (e.g., Häkkinen et al., 2011; Lohmann et al., 2009; Piecuch et al., 2017; Robson et al., 2012). Several studies have, for instance, previously related inflow changes to large-scale wind forcing associated with the NAO (e.g., Bringedal et al., 2018; Hansen & Østerhus, 2000; Sandø et al., 2012). In ECCOv4, the correlation between $HT\{v'\bar{\theta}\}$ and the NAO index is significant for the full time period (Figure 11; $r = 0.45$). However, this mostly reflects covariability during the 1990s, and the inflow variability appears not to have been driven by the NAO in the latter part of the time series (correlation not significant for 2000–2014). This supports the finding that the ocean circulation in the subpolar North Atlantic has been decoupled from the NAO in recent decades (Foukal & Lozier, 2017; Lohmann et al., 2009). The regression pattern between the Atlantic inflow strength and the barotropic stream function (Figure 10a) does, however, closely resemble the circulation anomalies associated with the EAP index (Figure 10b). The EAP reflects changes in the wind stress curl over the

subpolar North Atlantic (Barnston & Livezey, 1987) and is known to modulate ocean circulation in the subpolar North Atlantic (Foukal & Lozier, 2017; Häkkinen et al., 2011). For the ECCOv4 time period, the EAP reflects well the SPG strength (Figure 11; $r = -0.70$). Our results thus support a modulation of the gyre strength through wind stress curl variability associated with the EAP.

4. Discussion and Conclusions

In this study, a regional heat budget for the Norwegian Sea has been calculated using the ECCOv4 ocean state estimate in order to quantify the relative importance of ocean dynamics and local surface forcing. We find ocean advection and air-sea heat fluxes to be equally important in driving interannual heat content variability between 1993 and 2014, consistent with the findings of Mork et al. (2014). A further spatial analysis shows advection to be dominant (60–80%) in the Atlantic domain within the Norwegian Sea domain. While this dominance of advection in the Atlantic domain is along the lines of Carton et al. (2011), we note that, unlike Carton et al. (2011), our results suggest an active role of air-sea heat fluxes in generating heat anomalies also within the Atlantic domain. This discrepancy could be a result of the 2-year low-pass filter applied in Carton et al. (2011), which emphasizes multiannual variability more influenced by ocean advection (Buckley et al., 2014).

Spatial and temporal decompositions of the advection budget term show that non-Ekman dynamics dominate the advective heat transport in the region, consistent with the findings of Furevik and Nilsen (2005) and Raj et al. (2018). Furthermore, advection by Eulerian velocities dominates, while eddy-driven transports appear to have a dampening effect. The Atlantic water inflow is found to be a major source of the advection-driven convergence of heat within the Norwegian Sea domain (Figure 8a). However, we also find that the outflow regions are necessary to capture the correct magnitude and phase of the basin-scale heat anomalies (Figure 8b), suggesting that local surface forcing (air-sea heat fluxes and Ekman forcing) is important for modifying the anomalies along their poleward pathway. Furthermore, while velocity fluctuations are found to control heat transport variability at the Atlantic water inflow region, temperature fluctuations become increasingly more important at the outflow regions—a result that also points to surface forcing within the Norwegian Sea domain being important.

The ECCOv4 time period is relatively short, and, as highlighted in Mork et al. (2014), the relative amount of heat content change caused by ocean advection and air-sea heat fluxes is likely not stationary in time. For the Norwegian Sea this can for instance be a varying influence of the East Icelandic Current. In this paper we have focused on analyzing overall heat content variability for the ECCOv4 time period. It is, however, evident from our heat budget (Figure 4) that some of the warming/cooling events are purely advection driven (e.g., 2007), some are purely air-sea heat flux driven (e.g., 1999), and some are a mix of the two (e.g., 2002).

Our results indicate that the strength of the Atlantic inflow ($HT\{v'\bar{\theta}\}$) is related to ocean circulation variability in the subpolar North Atlantic, as expressed by the SPG strength—a strong/weak inflow being associated with a weak/strong gyre. Increased northward transport of Atlantic water in the northeastern Atlantic as a result of a weakened SPG is in agreement with previous studies (Häkkinen et al., 2011; Hátún et al., 2005). A weakened SPG is commonly associated with a northwest shift of the subpolar front, that is, a smaller gyre, allowing an increased northward advection of warm subtropical water into the eastern subpolar North Atlantic and Norwegian Sea (Hátún et al., 2005). However, in ECCOv4, changes in the strength of the gyre associated with increased Atlantic inflow to the Norwegian Sea are mostly confined to the western SPG region (Figure 10a), and not to a large degree related to the zonal extent of the gyre along the eastern boundary. Hence, the eastward expansions and contractions of the gyre do not control the strength of the Atlantic inflow to the Norwegian Sea.

In line with our results, heat budget estimates from the eastern subpolar North Atlantic, just upstream of the Norwegian Sea, find variations in ocean heat transport to be a major source of heat content variability (Desbruyères et al., 2015; Foukal & Lozier, 2018). These studies demonstrate that anomalous northward heat transport in the eastern subpolar North Atlantic is strongly influenced by the strength of the inter-gyre connection between the subtropical and SPGs. This is consistent with our finding of a wind-driven strengthening and northward shift of the North Atlantic Current when the Atlantic inflow to the Norwegian Sea is high (Figure 10; Marshall et al., 2001).

We note that unlike gyre indexes inferred from sea surface height (SSH; e.g., Häkkinen & Rhines, 2004; Hátún et al., 2005), the gyre strength in ECCOv4 (calculated directly from the barotropic stream function)

shows no decline in SPG circulation. The trend in the SSH-based SPG index comes from a basin-wide sea level rise in the North Atlantic (Foukal & Lozier, 2017; Hátún & Chafik, 2018), which does not translate into dynamical SPG changes. Constructing an SPG index based on detrended SSH in ECCOv4 yields similar gyre variations as to that obtained from the barotropic stream function ($r = 0.67$ if the SSH-based index leads by 1 year). For a recent, more detailed discussion on the calculation and interpretation of SSH-based SPG indexes, see Hátún and Chafik (2018).

The accuracy of the ECCOv4 ocean state estimate depends on the model fields being well constrained to actual observational data. The good match to observed variability in Norwegian Sea heat and freshwater content (Figure 2), and FSC and BSO temperatures (Figures 3c and 3d), implies a well-constrained ocean state estimate in our region of interest. As the Atlantic inflow strength is found to be a major source of Norwegian Sea heat content variability, the good fit to observed FSC volume transport is encouraging (Figure 3a), despite the poor representation of BSO transport variability (Figure 3b). The applied air-sea heat fluxes represent an additional source of uncertainty (Carton et al., 2011). However, ERA-Interim reanalysis, which provides ECCOv4 with its initial atmospheric state, has been shown to perform well in the Nordic Seas region (Lindsay et al., 2014). The mean turbulent heat fluxes calculated within the ECCOv4 framework are higher than in ERA-Interim (93 and 77 W/m^2, respectively, when averaged over the Norwegian Sea), but the variance (6 and 5 W/m^2) and interannual variability are similar ($r = 0.84$). As the effect of mesoscale eddies are largely parametrized, eddy-driven transport of heat could be underrepresented and thus lead to an elevated heat loss to the atmosphere. Lastly, although we have demonstrated the realism of ECCOv4 for our region of interest, our results are based on a single model, and the robustness of our results therefore need to be further established.

By performing a detailed heat budget analysis for the Norwegian Sea, we have identified an important role of ocean dynamics/nonlocal forcing in the Atlantic domain. This finding implies a potential for prediction of ocean heat content on interannual time scales, as skillful predictions of ocean heat content generally arise from the realistic initialization of ocean circulation anomalies associated with ocean dynamics (e.g., Yeager & Robson, 2017). Our results thus support and detail the findings from initialized climate prediction models, which demonstrate that large-scale circulation changes in the subpolar North Atlantic are communicated toward the Arctic via the Norwegian Sea (Langehaug et al., 2017; Yeager et al., 2015; Yeager & Robson, 2017). We find that interannual heat content anomalies in the Norwegian Sea are more related to the variable strength of the Atlantic water inflow than to temperature changes of the inflowing water. Observations nevertheless show that on multiannual to decadal time scales, temperature anomalies are able to propagate into and through the Norwegian Sea (Årthun et al., 2017; Broomé & Nilsson, 2018), something which suggests that temperature anomalies advected by the mean current could play a more important role in the heat budget on longer time scales. The time period covered by ECCOv4 is, however, too short to assess decadal variability in Norwegian Sea heat content. Our results furthermore highlight the importance of air-sea fluxes in generating and modifying ocean heat anomalies within the Norwegian Sea, which, at times, can mask the predictable oceanic variability. As the predictability of individual warming/cooling events is expected to vary depending on their dominant driver, heat budget diagnostics, such as those presented here, provide valuable benchmarks for assessing the skill of climate prediction models (e.g., Robson et al., 2012; Yeager et al., 2012).

Acknowledgments
The authors thank two anonymous reviewers for useful comments that improved the manuscript. This research was supported by the Research Council of Norway project PATHWAY (grant 263223), the Blue-Action project (European Union's Horizon 2020 research and innovation program, grant 727852), and the Trond Mohn Foundation (project number BFS2018TMT01). The ECCOv4 ocean state estimate is available at https://ecco.jpl.nasa.gov/products/all/ website. ERA-Interim reanalysis is available at https://www.ecmwf.int/en/forecasts/datasets/archive-datasets/reanalysis-datasets/era-interim website. Time series of Norwegian Sea heat and freshwater content and FSC temperature are available at https://ocean.ices.dk/iroc/ website. Volume transport estimates from the FSC were provided by Bee Berx, Marine Scotland, UK.

References

Årthun, M., & Eldevik, T. (2016). On anomalous ocean heat transport toward the Arctic and associated climate predictability. *Journal of Climate*, *29*(2), 689–704. https://doi.org/10.1175/JCLI-D-15-0448.1

Årthun, M., Eldevik, T., Smedsrud, L. H., Skagseth, Ø., & Ingvaldsen, R. B. (2012). Quantifying the influence of Atlantic heat on Barents sea ice variability and retreat. *Journal of Climate*, *25*(13), 4736–4743. https://doi.org/10.1175/JCLI-D-11-00466.1

Årthun, M., Eldevik, T., Viste, E., Drange, H., Furevik, T., Johnson, H. L., & Keenlyside, N. S. (2017). Skillful prediction of northern climate provided by the ocean. *Nature Communications*, *8*, 15875. https://doi.org/10.1038/ncomms15875

Barnston, A. G., & Livezey, R. E. (1987). Classification, seasonality and persistence of low-frequency atmospheric circulation patterns. *Monthly Weather Review*, *115*(6), 1083–1126. https://doi.org/10.1175/1520-0493(1987)115<1083:CSAPOL>2.0.CO;2

Berx, B., Hansen, B., Østerhus, S., Larsen, K. M., Sherwin, T., & Jochumsen, K. (2013). Combining in situ measurements and altimetry to estimate volume, heat and salt transport variability through the Faroe-Shetland Channel. *Ocean Science*, *9*(4), 639–654. https://doi.org/10.5194/os-9-639-2013

Bringedal, C., Eldevik, T., Skagseth, Ø., Spall, M. A., & Østerhus, S. (2018). Structure and forcing of observed exchanges across the Greenland-Scotland Ridge. *Journal of Climate*, *31*(24), 9881–9901. https://doi.org/10.1175/JCLI-D-17-0889.1

Broomé, S., & Nilsson, J. (2018). Shear dispersion and delayed propagation of temperature anomalies along the Norwegian Atlantic Slope Current. *Tellus A: Dynamic Meteorology and Oceanography*, *70*(1), 1453215. https://doi.org/10.1080/16000870.2018.1453215

Buckley, M. W., Ponte, R. M., Forget, G., & Heimbach, P. (2014). Low-frequency sst and upper-ocean heat content variability in the North Atlantic. *Journal of Climate*, *27*(13), 4996–5018. https://doi.org/10.1175/JCLI-D-13-00316.1

Buckley, M. W., Ponte, R. M., Forget, G., & Heimbach, P. (2015). Determining the origins of advective heat transport convergence variability in the North Atlantic. *Journal of Climate*, *28*(10), 3943–3956. https://doi.org/10.1175/JCLI-D-14-00579.1

Carton, J. A., Chepurin, G. A., Reagan, J., & Häkkinen, S. (2011). Interannual to decadal variability of Atlantic water in the Nordic and adjacent seas. *Journal of Geophysical Research*, *116*, C11035. https://doi.org/10.1029/2011JC007102

Chafik, L., Nilsson, J., Skagseth, Ø., & Lundberg, P. (2015). On the flow of Atlantic water and temperature anomalies in the Nordic Seas toward the Arctic Ocean. *Journal of Geophysical Research: Oceans*, *120*, 7897–7918. https://doi.org/10.1002/2015JC011012

Dee, D. P., Uppala, S. M., Simmons, A. J., Berrisford, P., Poli, P., Kobayashi, S., et al. (2011). The ERA-Interim reanalysis: Configuration and performance of the data assimilation system. *Quarterly Journal of the Royal Meteorological Society*, *137*(656), 553–597. https://doi.org/10.1002/qj.828

Desbruyères, D., Mercier, H., & Thierry, V. (2015). On the mechanisms behind decadal heat content changes in the eastern subpolar gyre. *Progress in Oceanography*, *132*, 262–272. https://doi.org/10.1016/J.POCEAN.2014.02.005

Dong, S., & Kelly, K. A. (2003). Heat budget in the gulf stream region: The importance of heat storage and advection. *Journal of Physical Oceanography*, *34*, 1214–1231. https://doi.org/10.1175/1520-0485(2004)034<1214:HBITGS>2.0.CO;2

Ebisuzaki, W. (1997). A method to estimate the statistical significance of a correlation when the data are serially correlated. *Journal of Climate*, *10*, 2147–2153. https://doi.org/10.1175/1520-0442(1997)010<2147:AMTETS>2.0.CO;2

Eldevik, T., Nilsen, J. E. Ø., Iovino, D., Anders Olsson, K., Sandø, A. B., & Drange, H. (2009). Observed sources and variability of Nordic seas overflow. *Nature Geoscience*, *2*(6), 406–410. https://doi.org/10.1038/ngeo518

Forget, G., Campin, J.-M, Heimbach, P., Hill, C. N., Ponte, R. M., & Wunsch, C. (2015a). ECCO version 4: An integrated framework for non-linear inverse modeling and global ocean state estimation. *Geoscientific Model Development*, *8*, 3071–3104. https://doi.org/10.5194/gmd-8-3071-2015

Forget, G., Ferreira, D., & Liang, X. (2015b). On the observability of turbulent transport rates by Argo: Supporting evidence from an inversion experiment. *Ocean Science*, *11*(5), 839–853. https://doi.org/10.5194/os-11-839-2015

Foukal, N. P., & Lozier, M. S. (2016). No inter-gyre pathway for sea-surface temperature anomalies in the North Atlantic. *Nature Communications*, *7*, 11333. https://doi.org/10.1038/ncomms11333

Foukal, N. P., & Lozier, M. S. (2017). Assessing variability in the size and strength of the North Atlantic subpolar gyre. *Journal of Geophysical Research: Oceans*, *122*, 6295–6308. https://doi.org/10.1002/2017JC012798

Foukal, N. P., & Lozier, M. S. (2018). Examining the origins of ocean heat content variability in the eastern North Atlantic subpolar gyre. *Geophysical Research Letters*, *45*, 11,275–11,283. https://doi.org/10.1029/2018GL079122

Fukumori, I., Wang, O., Fenty, I., Forget, G., Heimbach, P., & Ponte, R. M. (2017). ECCO version 4 release 3. 1721.1/110380.

Furevik, T. (2001). Annual and interannual variability of Atlantic Water temperatures in the Norwegian and Barents Seas: 1980–1996. *Deep Sea Research Part I: Oceanographic Research Papers*, *48*(2), 383–404. https://doi.org/10.1016/S0967-0637(00)00050-9

Furevik, T., & Nilsen, J. E. Ø. (2005). Large-scale atmospheric circulation variability and its impacts on the Nordic Seas Ocean Climate—A review. In H. Drange (Ed.), *The Nordic Seas: An integrated perspective, Geophysical Monograph Series* (Vol. 158, pp. 105–136). Washington, DC: American Geophysical Union. https://doi.org/10.1029/158GM09

Gent, P. R., & Mcwilliams, J. C. (1990). Isopycnal mixing in ocean circulation models. *Journal of Physical Oceanography*, *20*(1), 150–155. https://doi.org/10.1175/1520-0485(1990)020<0150:IMIOCM>2.0.CO;2

González-Pola, C., Larsen, K. M. H., Fratantoni, P., Beszczynska-Möller, A., & Hughes, S. L. (Eds.) (2018). ICES Report on Ocean Climate 2016. ICES Cooperative Research Report No. 339 (110 pp.). Copenhagen, Denmark. https://doi.org/10.17895/ices.pub.4069

Häkkinen, S., & Rhines, P. B. (2004). Decline of subpolar north atlantic circulation during the 1990s. *Science*, *304*(5670), 555–559. https://doi.org/10.1126/science.1094917

Häkkinen, S., Rhines, P. B., & Worthen, D. L. (2011). Warm and saline events embedded in the meridional circulation of the northern North Atlantic. *Journal of Geophysical Research*, *116*, C03006. https://doi.org/10.1029/2010JC006275

Hansen, B., & Østerhus, S. (2000). North Atlantic-Nordic Seas exchanges. *Progress in Oceanography*, *45*(2), 109–208. https://doi.org/10.1016/S0079-6611(99)00052-X

Hátún, H., & Chafik, L. (2018). On the recent ambiguity of the North Atlantic subpolar gyre index. *Journal of Geophysical Research: Oceans*, *123*, 5072–5076. https://doi.org/10.1029/2018JC014101

Hátún, H., Payne, M. R., Beaugrand, G., Reid, P. C., Sandø, A. B., Drange, H., et al. (2009). Large bio-geographical shifts in the north-eastern Atlantic Ocean: From the subpolar gyre, via plankton, to blue whiting and pilot whales. *Progress in Oceanography*, *80*, 149–162. https://doi.org/10.1016/j.pocean.2009.03.001

Hátún, H., Sandø, A. B., Drange, H., Hansen, B., & Valdimarsson, H. (2005). Influence of the Atlantic subpolar gyre on the thermohaline circulation. *Science*, *309*, 1841–1844. https://doi.org/10.1126/science.1114777

Heimbach, P., Hill, C., & Giering, R. (2005). An efficient exact adjoint of the parallel MIT General Circulation Model, generated via automatic differentiation. *Future Generation Computer Systems*, *21*(8), 1356–1371. https://doi.org/10.1016/J.FUTURE.2004.11.010

Hurrell, J. W. (1995). Decadal trends in the North Atlantic Oscillation: Regional temperatures and precipitation. *Science*, *269*(5224), 676–679. https://doi.org/10.1126/science.269.5224.676

Ingvaldsen, R., Loeng, H., & Asplin, L. (2002). Variability in the Atlantic inflow to the Barents Sea based on a one-year time series from moored current meters. *Continental Shelf Research*, *22*(3), 505–519. https://doi.org/10.1016/S0278-4343(01)00070-X

Isachsen, P. E., Koszalka, I., & LaCasce, J. H. (2012). Observed and modeled surface eddy heat fluxes in the eastern Nordic Seas. *Journal of Geophysical Research*, *117*, C08020. https://doi.org/10.1029/2012JC007935

Jungclaus, J. H., Lohmann, K., & Zanchettin, D. (2014). Enhanced 20th-century heat transfer to the Arctic simulated in the context of climate variations over the last millennium. *Climate of the Past*, *10*, 2201–2213. https://doi.org/10.5194/cp-10-2201-2014

Krahmann, G., Visbeck, M., & Reverdin, G. (2001). Formation and propagation of temperature anomalies along the North Atlantic Current. *Journal of Physical Oceanography*, *31*(5), 1287–1303. https://doi.org/10.1175/1520-0485(2001)031<1287:FAPOTA>2.0.CO;2

Langehaug, H. R., Matei, D., Eldevik, T., Lohmann, K., & Gao, Y. (2017). On model differences and skill in predicting sea surface temperature in the Nordic and Barents Seas. *Climate Dynamics*, *48*(3-4), 913–933. https://doi.org/10.1007/s00382-016-3118-3

Langehaug, H. R., Medhaug, I., Eldevik, T., & Otterå, O. H. (2012). Arctic/atlantic exchanges via the subpolar gyre. *Journal of Climate*, *25*(7), 2421–2439. https://doi.org/10.1175/JCLI-D-11-00085.1

Large, W., & Yeager, S. G. (2004). Diurnal to decadal global forcing for ocean and sea-ice models: The data sets and flux climatologies, (Tech. Rep.). https://doi.org/10.5065/D6KK98Q6

Lee, T., Fukumori, I., & Tang, B. (2004). Temperature advection: Internal versus External Processes. *Journal of Physical Oceanography*, *34*(8), 1936–1944. https://doi.org/10.1175/1520-0485(2004)034<1936:TAIVEP>2.0.CO;2

Lien, V. S., Gusdal, Y., & Vikebø, F. B. (2014). Along-shelf hydrographic anomalies in the Nordic Seas (1960-2011): Locally generated or advective signals? *Ocean Dynamics*, *64*(7), 1047–1059. https://doi.org/10.1007/s10236-014-0736-3

Lien, V. S., Hjøllo, S. S., Skogen, M. D., Svendsen, E., Wehde, H., Bertino, L., et al. (2016). An assessment of the added value from data assimilation on modelled Nordic Seas hydrography and ocean transports. *Ocean Modelling*, *99*, 43–59. https://doi.org/10.1016/j.ocemod.2015.12.010

Lindsay, R., Wensnahan, M., Schweiger, A., & Zhang, J. (2014). Evaluation of seven different atmospheric reanalysis products in the Arctic. *Journal of Climate*, *27*(7), 2588–2606. https://doi.org/10.1175/JCLI-D-13-00014.1

Lohmann, K., Drange, H., & Bentsen, M. (2009). A possible mechanism for the strong weakening of the North Atlantic subpolar gyre in the mid-1990s. *Geophysical Research Letters*, *36*, L15602. https://doi.org/10.1029/2009GL039166

Marshall, J., Johnson, H., & Goodman, J. (2001). A study of the interaction of the North Atlantic Oscillation with ocean circulation. *Journal of Climate*, *14*(7), 1399–1421. https://doi.org/10.1175/1520-0442(2001)014<1399:ASOTIO>2.0.CO;2

Mork, K. A., Skagseth, Ø., Ivshin, V., Ozhigin, V., Hughes, S. L., & Valdimarsson, H. (2014). Advective and atmospheric forced changes in heat and fresh water content in the Norwegian Sea, 1951–2010. *Geophysical Research Letters*, *41*, 6221–6228. https://doi.org/10.1002/2014GL061038

Mosby, H. (1962). Water, salt and the heat balance of the North Polar Sea and of the Norwegian Sea. *Geophysica Norvegica*, *24*, 289–313.

Nilsen, F., Gjevik, B., & Schauer, U. (2006). Cooling of the west spitsbergen current: Isopycnal diffusion by topographic vorticity waves. *Journal of Geophysical Research*, *111*, C08012. https://doi.org/10.1029/2005JC002991

Nurser, A. J. G., & Bacon, S. (2014). The Rossby radius in the Arctic Ocean. *Ocean Science*, *10*(6), 967–975. https://doi.org/10.5194/os-10-967-2014

Orvik, K. A., & Niiler, P. (2002). Major pathways of Atlantic water in the northern North Atlantic and Nordic Seas toward Arctic. *Geophysical Research Letters*, *29*(19), 1896. https://doi.org/10.1029/2002GL015002

Orvik, K. A., & Skagseth, Ø. (2005). Heat flux variations in the eastern Norwegian Atlantic Current toward the Arctic from moored instruments. *Geophysical Research Letters*, *32*, L14610. https://doi.org/10.1029/2005GL023487

Piecuch, C. G., & Ponte, R. M. (2012). Importance of circulation changes to atlantic heat storage rates on seasonal and interannual time scales. *Journal of Climate*, *25*(1), 350–362. https://doi.org/10.1175/JCLI-D-11-00123.1

Piecuch, C. G., Ponte, R. M., Little, C. M., Buckley, M. W., & Fukumori, I. (2017). Mechanisms underlying recent decadal changes in subpolar North Atlantic Ocean heat content. *Journal of Geophysical Research: Oceans*, *122*, 7181–7197. https://doi.org/10.1002/2017JC012845

Poulain, P.-M., Warn-Varnas, A., & Niiler, P. P. (1996). Near-surface circulation of the Nordic Seas as measured by Lagrangian drifters. *Journal of Geophysical Research*, *101*(C8), 18,237–18,258. https://doi.org/10.1029/96JC00506

Raj, R. P., Nilsen, J. E., Johannessen, J. A., Furevik, T., Andersen, O. B., & Bertino, L. (2018). Quantifying Atlantic water transport to the Nordic seas by remote sensing. *Remote Sensing of Environment*, *216*, 758–769. https://doi.org/10.1016/J.RSE.2018.04.055

Rio, M.-H., & Hernandez, F. (2003). High-frequency response of wind-driven currents measured by drifting buoys and altimetry over the world ocean. *Journal of Geophysical Research*, *108*(C8), 3283. https://doi.org/10.1029/2002JC001655

Robson, J. I., Sutton, R. T., & Smith, D. M. (2012). Initialized decadal predictions of the rapid warming of the North Atlantic Ocean in the mid 1990s. *Geophysical Research Letters*, *39*, L19713. https://doi.org/10.1029/2012GL053370

Sandø, A. B., Nilsen, J. E. Ø., Eldevik, T., & Bentsen, M. (2012). Mechanisms for variable North Atlantic-Nordic seas exchanges. *Journal of Geophysical Research*, *117*, C12006. https://doi.org/10.1029/2012JC008177

Saravanan, R., & McWilliams, J. C. (1998). Advective ocean-atmosphere interaction: An analytical stochastic model with implications for decadal variability. *Journal of Climate*, *11*(2), 165–188. https://doi.org/10.1175/1520-0442(1998)011<0165:AOAIAA>2.0.CO;2

Schauer, U., & Beszczynska-Möller, A. (2009). Problems with estimation and interpretation of oceanic heat transport–Conceptual remarks for the case of Fram Strait in the Arctic Ocean. *Ocean Science*, *5*, 487–494.

Schauer, U., Fahrbach, E., Osterhus, S., & Rohardt, G. (2004). Arctic warming through the Fram Strait: Oceanic heat transport from 3 years of measurements. *Journal of Geophysical Research*, *109*, C06026. https://doi.org/10.1029/2003JC001823

Segtnan, O. H., Furevik, T., & Jenkins, A. D. (2011). Heat and freshwater budgets of the Nordic seas computed from atmospheric reanalysis and ocean observations. *Journal of Geophysical Research*, *116*, C11003. https://doi.org/10.1029/2011JC006939

Sherwin, T. J., Williams, M. O., Turrell, W. R., Hughes, S. L., & Miller, P. I. (2006). A description and analysis of mesoscale variability in the Färoe-Shetland Channel. *Journal of Geophysical Research*, *111*, C03003. https://doi.org/10.1029/2005JC002867

Simonsen, S. K., & Haugan, P. M. (1996). Heat budgets of the Arctic Mediterranean and sea surface heat flux parameterizations for the Nordic Seas. *Journal of Geophysical Research*, *101*(15), 6553–6576. https://doi.org10.1029/95JC03305

Skagseth, Ø., Furevik, T., Ingvaldsen, R., Loeng, H., Mork, K. A., Orvik, K. A., & Ozhigin, V. (2008). Volume and heat transports to the Arctic Ocean via the Norwegian and Barents Seas, *Arctic-subarctic ocean fluxes* (pp. 45–64). Dordrecht, Netherlands: Springer. https://doi.org/10.1007/978-1-4020-6774-7_3

Sutton, R. T., & Allen, M. R. (1997). Decadal predictability of North Atlantic sea surface temperature and climate. *Nature*, *388*, 563–567. https://doi.org/:10.1038/41523

Wunsch, C., & Heimbach, P. (2007). Practical global oceanic state estimation. *Physica D*, *230*, 197–208. https://doi.org/10.1016/j.physd.2006.09.040

Yeager, S. G., Karspeck, A. R., & Danabasoglu, G. (2015). Predicted slowdown in the rate of Atlantic sea ice loss. *Geophysical Research Letters*, *42*, 704–10. https://doi.org/10.1002/2015GL065364

Yeager, S., Karspeck, A., Danabasoglu, G., Tribbia, J., & Teng, H. (2012). A decadal prediction case study: Late twentieth-century north atlantic ocean heat content. *Journal of Climate*, *25*, 5173–5189. https://doi.org/10.1175/JCLI-D-11-00595.1

Yeager, S. G., & Robson, J. I. (2017). Recent progress in understanding and predicting atlantic decadal climate variability. *Current Climate Change Reports*, *3*(2), 112–127. https://doi.org/10.1007/s40641-017-0064-z

Zhao, J., Bower, A., Yang, J., Lin, X., & Penny Holliday, N. (2018). Meridional heat transport variability induced by mesoscale processes in the subpolar North Atlantic. *Nature Communications*, *9*(1), 1124. https://doi.org/10.1038/s41467-018-03134-x